Supporting Information

"All-Three-in-One": A New Bismuth-Tellurium-Borate Bi_3TeBO_9 Exhibiting Strong Second Harmonic Generation Response

Mingjun Xia,[†] Xingxing Jiang,[†] Zheshuai Lin[*,†,‡] and Rukang Li[†,‡]*

[†]*Beijing Center for Crystal Research and Development, Key Laboratory of Functional Crystals and Laser Technology, Technical Institute of Physics and Chemistry, Chinese Academy of Sciences, Beijing 100190, China.*

[‡]*University of Chinese Academy of Sciences, Beijing 100049, China.*

Contents：

11. Reference

1. Powder X-ray diffraction: The powder X-ray diffraction (PXRD) data were collected on a Bruker D8 Focus diffractometer equipped with Cu Kα radiation (λ = 1.5418 Å) at room temperature in the 2θ range of 7 - 70^{o}. The Rietveld refinement of PXRD patterns of BTBO samples was conducted to confirm the phase purities using GSAS and EXPGUI software programs.[1, 2]

2. Single crystal structure determination: A Bi_3TeBO_9 crystal with the dimensions of 0.06 × 0.05 × 0.035 mm^3 was chosen for single crystal X-ray diffraction measurement. The crystal data were collected by using graphite-monochromated Mo Kα radiation (λ = 0.71073Å) on a Bruker APEX II single crystal X-ray diffractometer at room temperature. The structure was solved with direct method by program SHELXS-97 and refined by the full matrix least squares on F^2 by SHELXL-97, respectively.[3] All atoms were refined with anisotropic displacement parameters. The crystal structure was verified by the ADDSYM algorithm using program PLATON[4] and no additional symmetry was given. The crystallographic data and refinement are summarized in Table S1. The atomic coordinates, equivalent displacement parameters and bond valence sums (BVS) are given in Table S2. The selected bond lengths and angles are presented in Table S3.

3. Thermal analysis: The differential scanning calorimetric (DSC) analysis was performed on a Labsys^{TM} TG – DTA16 (SETARAM) thermal analyzer under nitrogen gas flow. The samples was heated from room temperature to 900 ^{o}C at a rate of 15 ^{o}C per minute and then cooled to room temperature at the same rate.

4. UV-VIS-NIR diffuse reflectance spectrum: The diffuse reflectance spectrum was measured on a Varian Cary 5000 spectrophotometer fitted with an integrating sphere in the wavelength range from 200 nm to 2500 nm with $BaSO_4$ used as a reference material (100% reflectance). The absorption (α/S) spectra were converted from reflectance spectra according to the following Kubelka-Munk function: $\alpha/S = (1-R)^2/2R$, where α, S and R is the absorption, scattering and reflectance coefficient, respectively.[5]

5. Infrared spectrum: Infrared (IR) spectroscopy was performed to specify the coordination of boron in BTBO. IR spectra were collected on a Varian Excalibur

3100 spectrometer in the 400 – 4000 cm^{-1} range. BTBO and dried KBr samples with mass ratio about 1:100 were weighed and mixed thoroughly.

5. SHG measurement: The SHG measurements of polycrystalline samples were performed with a Nd: YAG (λ = 1064 nm) as the incident light source. Bi_3TeBO_9 samples were ground and sieved into seven distinct size ranges, 20–50, 50–75, 75–100, 100–120, 120–150, 150-200 and 200–300 mm for the test. KDP was served as the reference and sieved into the same size ranges. The SHG signals from samples were detected by a photomultiplier tube.

6. Computational methods: The first-principles calculations are performed using CASTEP,[6] a plane-wave pseudopotential total energy package based on density functional theory (DFT).[7] Optimized norm-conserving pseudopotentials[8] in Kleinman-Bylander[9] form are employed to model the electron-ion interactions in Bi_3TeBO_9 and allow for the use of a relatively small plane-wave basis set without compromising the accuracy required by this study. The Perdew-Burke-Ernzerhof functionals[10] in generalized gradient approximation (GGA) form[11] is adopted to describe the exchange and correlation energy. A high kinetic energy cutoff of 800eV and dense Monkhorst-Pack[12] k-point meshes spanning less than 0.04 $Å^{-1}$ in the Brillouin zones are chosen. Tests show that these computational parameters give results that are sufficiently accurate for present purposes.

Due to the discontinuous nature of the exchange-correlation functional, the GGA-calculated band gap is smaller than the experimental value. Therefore, scissor operator[13] is adopted to raise all the conduction bands to match the calculated band gaps with the measured ones. Based on the scissor-corrected electronic band structure, the imaginary part of the dielectric function can be obtained from the electron transition between the valence band and conduction band.[14] Accordingly, the real part of the dielectric function can be determined using the Kramers-Kronig transform, and the theoretical refractive index (n) can be determined. Moreover, the SHG coefficients are calculated using expressions developed by Lin *et al*.[15]

Furthermore, to analyze the contribution of the three groups to the SHG coefficient, SHG-weighted electron density analysis[16] and real-space atom-cutting

technique[15] are employed. In SHG-weighted electron density analysis, the considered SHG coefficient is "resolved" onto each orbital or band, and then the SHG-weighted bands are used to sum the probability densities of all occupied (valence) or unoccupied (conduction) states. This ensures that the quantum states irrelevant to SHG are not shown in the occupied or unoccupied "SHG-densities," while the orbitals vital to SHG are intuitively highlighted in the real space. In real-space atom-cutting technique, the contribution of ion *A*, $\chi(A)$, to the optical coefficients is acquired by excluding all the atoms from the original wave function except *A*, *i.e.*, $\chi(A) = \chi$(all atoms excluded except *A*).

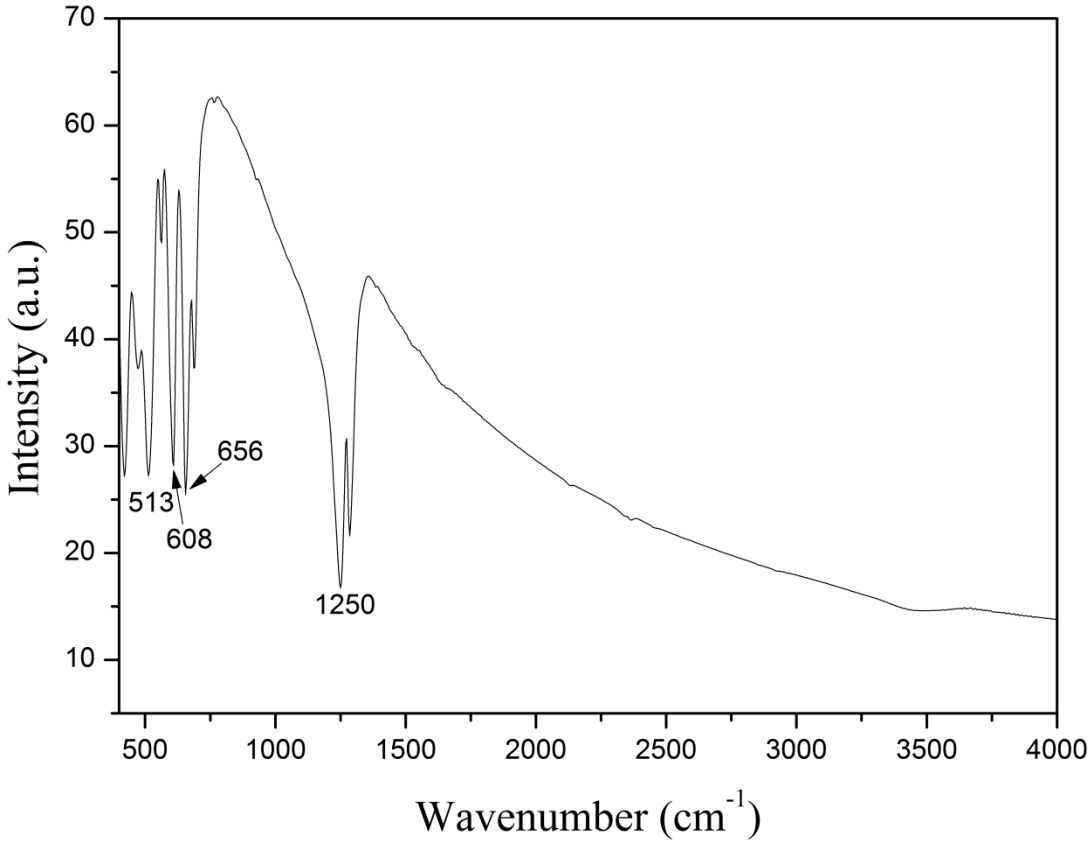

Figure S1. Infrared spectrum of Bi_3TeBO_9.

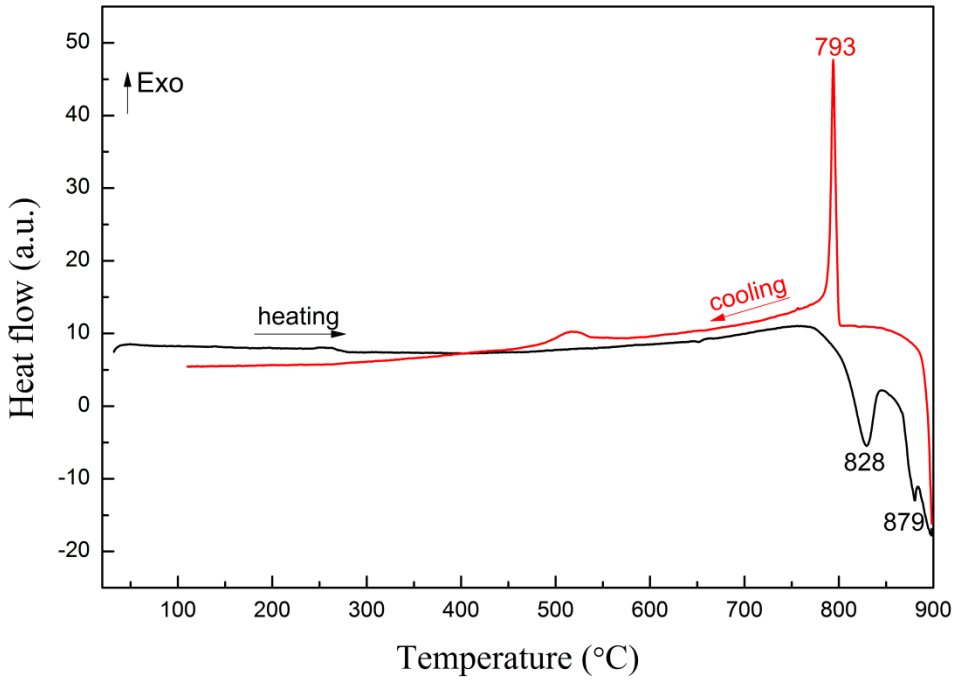

Figure S2. The DSC curves of Bi_3TeBO_9.

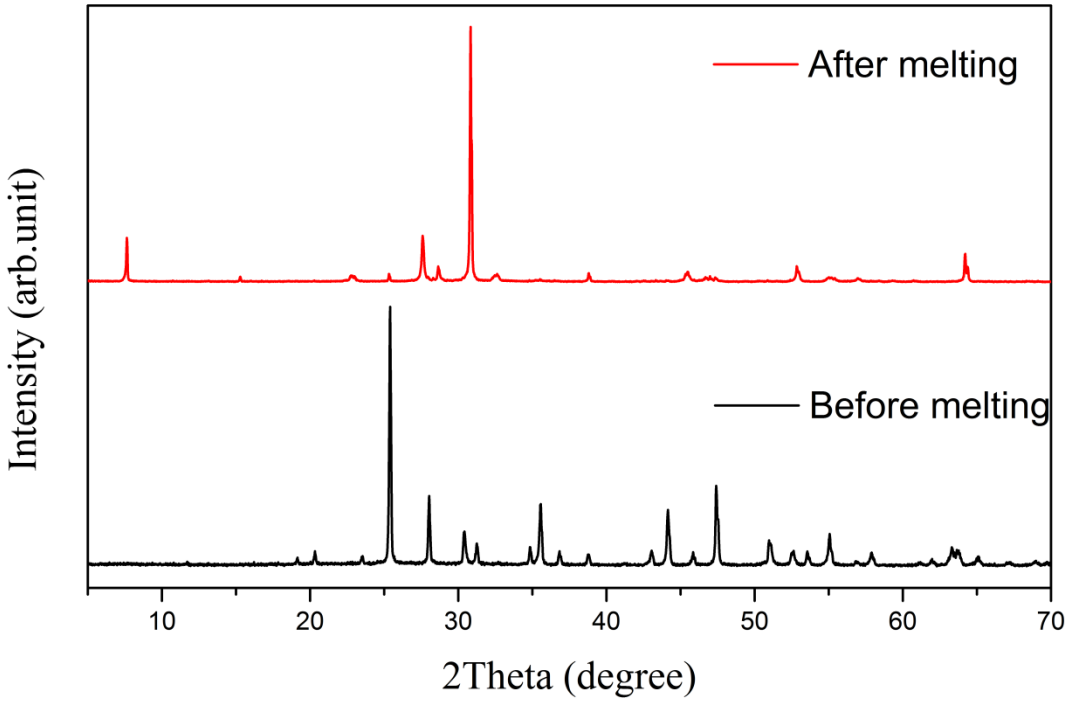

Figure S3. The XRD patterns of Bi_3TeBO_9 before and after melting.

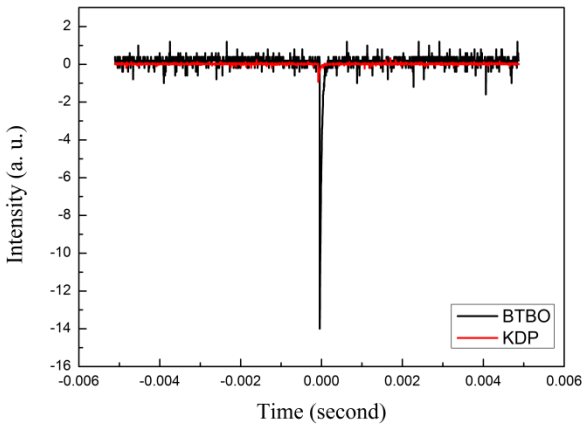

Figure S4. Oscilloscope traces of the SHG signals of KDP and Bi_3TeBO_9 at the powder size of 200 – 300 μm.

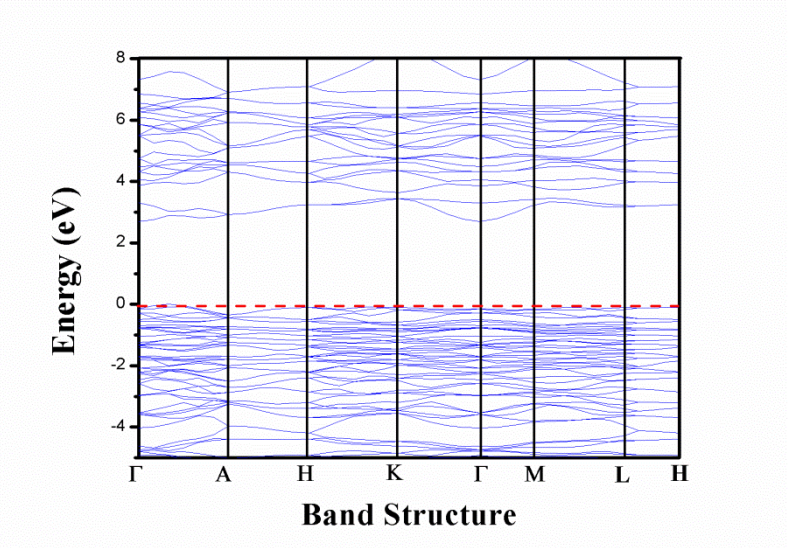

Figure S5. Electronic band structures along highly symmetrical path in the Brillouin zone for Bi_3TeBO_9.

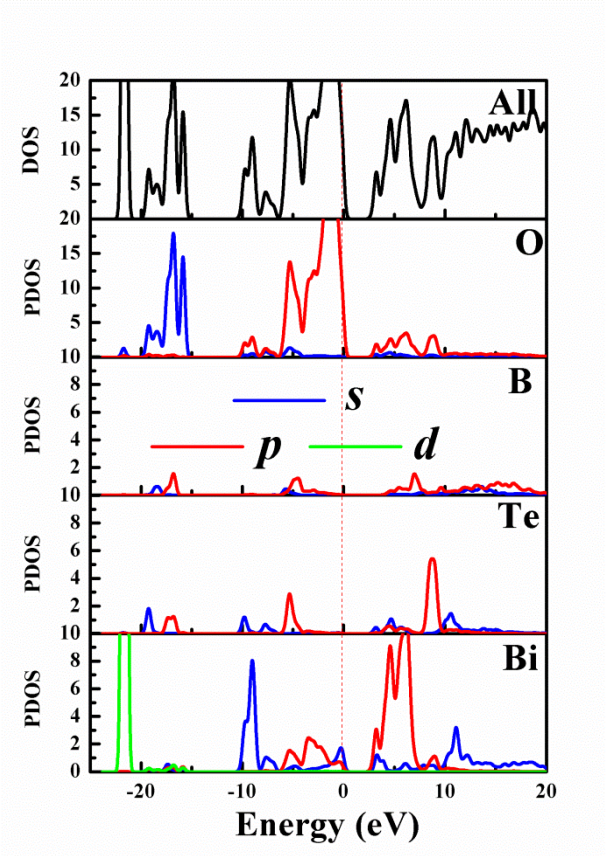

Figure S6. The partial density of state projected onto constitute atoms in Bi_3TeBO_9.

The Characteristics of the electronic structure are shown in Discussion S1.

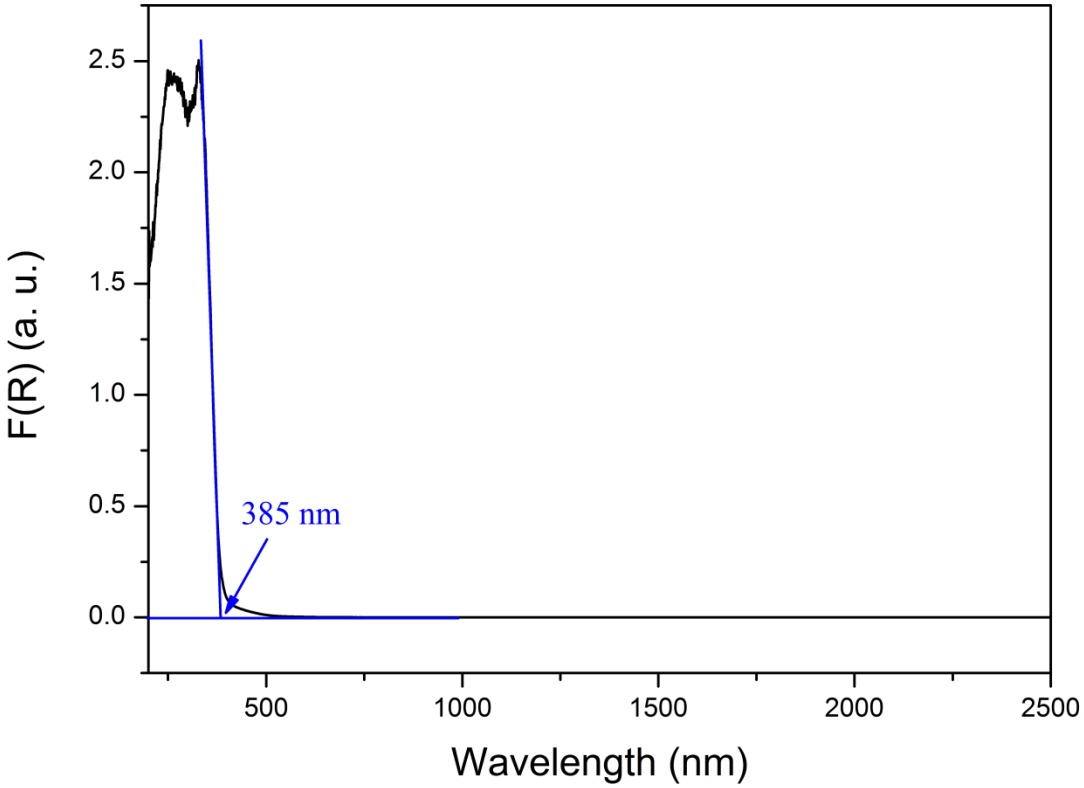

Figure S7. The UV-VIS-IR reflectance spectrum of Bi_3TeBO_9.

Table S1. Crystal data and structure refinement for Bi_3TeBO_9.

Formula	Bi_3TeBO_9
Wavelength (Å)	0.71073
Crystal system	Hexagonal
Space group	$P6_3$ (No.173)
a (Å)	8.7510(12)
c (Å)	5.8981(12)
Z	2
Volume ($Å^3$)	391.16(11)
Density (g/cm^3)	7.721
Absorption coefficient (mm^{-1})	70.998
F(000)	756
Goodness-of-fit on F^2	0.985
Absolute structure parameter	0.021(15)
Final R indices [I>2σ(I)][a]	R1 = 0.0250, wR2 = 0.0465
R indices (all data)[a]	R1 = 0.0275, wR2 = 0.0469
Extinction coefficient	0.0068(3)
Largest diff. peak and hole (e $Å^{-3}$)	2.101 and -2.696

[a] $R1 = \sum\big||F_O| - |F_C|\big|/\sum|F_O|;\ wR2 = \{\sum[w(F_O^2 - F_C^2)^2]/\sum[w(F_O^2)^2]\}^{1/2}$.

Table S2. Atomic coordinates, equivalent isotropic displacement parameters ($Å^2$) and bond valence sums (BVS) for Bi_3TeBO_9. U_{eq} is defined as one third of the trace of the orthogonalized U_{ij} tensor.

Atom	x	y	z	U_{eq}	BVS
Bi1	0.29827(3)	0. 34622(3)	0. 10689(12)	0.00170(9)	2.96
Te1	2/3	1/3	0.0813(2)	0.0007(2)	5.91
O1	0. 4599(9)	0. 2464(9)	0. 2679(12)	0.0035(13)	2.041
O2	0. 5407(8)	0. 4147(8)	-0. 1042(13)	0.0034(14)	1.929
O3	0. 1009(9)	0. 1813(8)	0. 4333(13)	0.0032(12)	1.941
B1	0	0	0.425(3)	0.005(4)	2.943

Table S3. Selected bond lengths (Å) and angles (deg) for Bi_3TeBO_9.

Bi1-O1	2.214(7)	Te1-O2^{iv}	1.924(7)
Bi1-O3^{i}	2.264(7)	Te1-O2^{v}	1.924(7)
Bi1-O2	2.267(7)	Te1-O2	1.924(7)
Bi1-O1^{ii}	2.505(7)	B1-O3	1.378(6)
Bi1-O3	2.506(7)	B1-O3^{vi}	1.378(6)
Bi1-O2^{iii}	2.514(7)	B1-O3^{vi}	1.378(6)
Te1-O^{iv}	1.921(7)	O3^{vi}-B1-O3	119.88(10)
Te1-O1^{v}	1.921(7)	O3^{vi}-B1-O3^{vii}	119.88(10)
Te1-O1	1.921(7)	O3-B1-O3^{vii}	119.88(10)

Symmetry transformations used to generate equivalent atoms: (i) y,-x+y,z-1/2; (ii) x-y,x,z-1/2; (iii) -x+1,-y+1,z+1/2; (iv) -y+1,x-y,z; (v) -x+y+1,-x+1,z; (vi) -y,x-y,z; (vii) -x+y,-x,z

Table S4. Comparison of the SHG effects among the common borate NLO crystals and Bi_3TeBO_9.

Crystal	Space Group	Powder SHG (× KDP)	References
LiB_3O_5 (LBO)	*P*na2_1	3 (d_{32} = 0.85 pm/V)	[17]
β-BaB_2O_4 (BBO)	*R*3m	4 (d_{22} = 1.6 pm/V)	[17]
CsB_3O_5 (CBO)	$P2_12_12_1$	3 (d_{14} = 1.04 pm/V)	[17]
$CsLiB_6O_{10}$ (CLBO)	$I\bar{4}$2d	3 (d_{36} = 0.95 pm/V)	[17]
$KBe_2BO_3F_2$ (KBBF)	*R*32	1.2(d_{11} = 0.47 pm/V)	[17]
$YCa_4O(BO_3)_3$	*C*m	1.5 (d_{33} = 1.24 pm/V*)	[17]
$BiCd_4O(BO_3)_3$	*C*m	6 (d_{11} = 3.21 pm/V*)	[18]
BiB_3O_6 (BIBO)	*C*2	5 (d_{22} = 2.95 pm/V*)	[18]
Bi_3TeBO_9	$P6_3$	~ 20 (d_{33} = 5.10 pm/V*)	This work

*Calculated values

Table S5. Flexibility index F of CdO_n (n = 6, 7) in $BiCd_4O(BO_3)_3$ and TeO_6 in $A_3M_3TeX_2O_{14}$ (A = Pb, Ba, Sr, M = Mg, Zn and X = P, V)[19] and Bi_3TeBO_9. The SHG coefficients of CdO_n or TeO_6 groups (d_{ij}/group) calculated by the real-space atom-cutting method are also listed for comparison. Clearly, the flexibility indices of TeO_6 is larger than CdO_n polyhedra, in consistent with the results of the atom-cutting calculations. The discussion on the physical mechanism of flexibility index is shown in Discussion S2.

Crystal	Unit	F	d_{ij}/group*
$BiCd_4O(BO_3)_3$	CdO_6	0.119	0.38 pm/V
$BiCd_4O(BO_3)_3$	CdO_7	0.090	0.13 pm/V
$Pb_3Zn_3TeP_2O_{14}$	TeO_6	0.154	2.33 pm/V
$Pb_3Zn_3TeV_2O_{14}$	TeO_6	0.151	2.25 pm/V
$Ba_3Zn_3TeP_2O_{14}$	TeO_6	0.152	1.86 pm/V
$Sr_3Zn_3TeP_2O_{14}$	TeO_6	0.154	1.98 pm/V
$Pb_3Mg_3TeP_2O_{14}$	TeO_6	0.153	2.08 pm/V
Bi_3TeBO_9	TeO_6	0.152	2.17 pm/V

*The values are normalized with respect to the spatial density of TeO_6 groups in Bi_3TeBO_9.

Discussion

Discussion S1. Characteristics of the electronic structure in Bi_3TeBO_9

The electronic band structure along highly symmetrical path of Bi_3TeBO_9 is displayed in Figure S4. Bi_3TeBO_9 is typical indirect band gap semiconductor with calculated band gap 2.70 eV, smaller than the experimental value (3.23 eV) by 0.53eV. The partial density of state projected onto constitute atoms is displayed in figure S5, and some characteristic can be deduced:(1) Bi *5d* orbital is strongly localized the energy states below -20 eV, which is difficult to be stimulated by external light electric field and contribute little to the optical property. Moreover, these orbitals hybridize little with the orbitals of other element, implying that they hardly participate in the formation of chemical bond. (2) The energy level between -20eV and -10eV mainly constitute of Bi *6s*, Te *5s 5p*, B *2s 2p* and O 2s orbitals, the strongly hybridization among these orbitals demonstrate the strong covalent bonds in BiO_6, TeO_6 and BO_3 groups. (3) In the top of the valence bands (-10 to 0 eV) and bottom of conduction bands (2.70 to 10 eV), the electron energy states mainly originates from Bi *6s 6p*, Te 5s 5p, B *2s 2p* and O *2p* orbitals. The optical property of crystal is dominantly determined by the electron transition across the forbidden, so all the three types group contributes to the SHG coefficient. And especially, the contribution of orbitals in BiO_6 octahedron is larger than TeO_6 octahedron and BO_3 triangle, implying that the contribution to SHG coefficient of former is larger than the latter.

Discuss S2. Physical mechanism of flexibility index

Flexibility index was proposed to characterize the induced polarizability by valence electrons[20]. It is known that the polarizability is the result of all electrons (including valence electrons and inner electrons) and nucleus. However, the inner electrons are always localized in deep energy level and do not participate in the chemical bond, and their energy states are hardly affected by external photoelectric field. For nucleus the responding spectrum are usually located at middle- or far-IR spectral region (with the wavelength usually larger than 3μm) due to their large mass. Thus, the contribution from nucleus to the polarizability is negligibly small when the alternating photoelectric field is in the near-IR, visible and UV regions. Thus, the induced polarization from valence electrons would have the dominant contribution to the linear and nonlinear optical properties in the near-IR, visible and UV NLO materials. In the 1970s, Levine proposed a "bond charge model", in which only the contribution of the bond charges (which are mainly constructed by valence electrons) is taken into consideration while that of the inner electrons and nucleus is ignored. Using this model, the good agreement between the calculated and experimental second-order susceptibilities was achieved.[20-22] Moreover, in recent years the plane-wave pseudopotential method based on density functional theory has been successfully applied to theoretically determine the nonlinear susceptibility of materials.[23-26] In this method, the potentials of inner electrons and nucleus are approximated by pseudopotentials, and only the valence electrons are used to obtain the electronic structures, from which the nonlinear optical coefficients are calculated.[15] The success of both methods implies that the nonlinear susceptibility is mainly arise from the polarizability of valence electrons, and the contribution of inner electrons and nucleus is very small and can be ignored. Namely, the "flexibility index" which only considers the contribution of valence electrons is valid for the SHG studies, although some approximations are adopted in this simple model.

The structures of $BiCd_4O(BO_3)_3$ and Bi_3TeBO_9 both contain the BiO_6 and BO_3 groups. Thus, it is anticipated that in some extends the very different SHG effects in

these two materials would arise from the difference of second-order Jahn-Teller distorted octahedra, CdO_n in $BiCd_4O(BO_3)_3$ and TeO_6 in Bi_3TeBO_9. The flexibility index calculations reveal that TeO_6 octahedra are more "flexible" than CdO_n polyhedra, indicating that the former groups are easier to generate the larger induced polarization compared with the latter. It is the more "flexible" ability of TeO_6 groups, combined with their higher spatial density (and higher spatial density of BiO_6 groups), that makes the SHG response significantly enhanced from $BiCd_4O(BO_3)_3$ (d_{33} = 3.21 pm/V) to Bi_3TeBO_9 (d_{33} = 5.10 pm/V).

Reference:

(1) Larson, A. C.; von Dreele, R. B. *General Structure Analysis System*, Los Alamos National Lab, 1994.

(2) Toby, B. H. *J. Appl. Crystallogr.* **2001**, *34*, 210-213.

(3) Sheldrick, G. M. *Acta Crystallogr. A* **2008**, *64*, 112.

(4) Spek, A. L. *J. Appl. Crystallogr.* **2003**, *36*, 7.

(5) Kubelka, P. *Z. Tech. Phys.* **1931**, *12*, 593

(6) Clark, S. J.; Segall, M. D.; Pickard, C. J.; Hasnip, P. J.; Probert, M. J.; Refson, K.; Payne, M. C. *Z. Kristallogr*. **2005**, *220*, 567.

(7) (a) Kohn, W., Sham, L. J. *Phys. Rev*. **1965**, *140*, 1133. (b) Payne, M. C.; Teter, M. P.; Allan, D. C.; Arias, T. A.; Joannopoulos, J. D. *Rev. Mod. Phys*. **1992**, *64*, 1045.

(8) Rappe, A. M.; Rabe, K. M.; Kaxiras, E.; Joannopoulos, J. D. *Phys. Rev. B*. **1990**, *41*, 1227.

(9) Kleinman, L.; Bylander, D. M. *Phys. Rev. Lett*. **1982**, *48*, 1425.

(10) Perdew, J. P.; Burke, K.; Ernzerhof, M. *Phys. Rev. Lett*. **1996**, *77*, 3865.

(11) Perdew, J. P.; Chevary, J. A.; Vosko, S. H.; Jackson, K. A.; Pederson, M. R.; Singh, D. J.; Fiolhais, C. *Phys. Rev. B*. **1992**, *46*, 6671.

(12) Monkhorst, H. J.; Pack, J. D. *Phys. Rev. B*. **1976**, *13*, 5188.

(13) Godby, R. W.; Schluter, M.; Sham, L. J. *Phys. Rev. B*. **1988**, 37, 10159.

(14) Palik, E. D. *Handbook of Optical Constants of Solids*, Academic Press, New York **1985**.

(15) Lin, J.; Lee, M. H.; Liu, Z. P.; Chen, C. T.; Pickard, C. J. *Phys. Rev. B*. **1999**, *60*, 13380.

(16) Lee, M. H.; Yang, C. H.; Jan, J. H. *Phys. Rev. B*. **2004**, *70*, 235110.

(17) Chen, C. T.; Sasaki, T.; Li, R. K.; Wu, Y. C.; Lin, Z. S.; Mori, Y.; Hu, Z. G.; Wang, J. Y.; Uda, S.; Yoshimura, M.; Kaneda, Y. *Nonlinear Optical Borate Crystals: Principles and Applications*. Wiley-VCH, **2012**.

(18) Zhang, W. L.; Cheng, W. D.; Zhang, H.; Geng, L.; Lin, C. S.; He, Z. Z. *J. Am. Chem. Soc*. **2010**, *132*, 1508.

(19) (a) Yu, H. W.; Zhang, W. G.; Young, J.; Rondinelli, J. M.; Halasyamani, P. S. *J. Am. Chem. Soc*. **2016**, *138*, 88. (b) Yu, H. W.; Young, I.; Wu, H. P.; Zhang, W. G.; Rondinelli, J. M.; Halasyamani, P. S. *J. Am. Chem. Soc*. **2016**, *138*, 4984.

(20) Levine. B. F. *Phys. Rev. Lett.* 1969, **22**, 787.

(21) Levine. B. F. *Phys. Rev. Lett.* 1970, **25**, 440.

(22) Levine. B. F. *Phys. Rev. B* 1973, **7**, 2600.

(23) Lin, Z. S.; Jiang, X. X.; Kang, L.; Gong, P. F.; Luo, S. Y.; Lee, M. H. *J. Phys. D: Appl. Phys*. **2014**, *47*, 253001.

(24) Zhao, S. G.; Gong, P. F.; Luo, S. Y.; Bai, L.; Lin, Z. S.; Ji, C. M.; Chen, T. L.; Hong, M. C.; Luo. J. H.; *J. Am. Chem. Soc*. **2014**, *136*, 8560.

(25) Kang, L.; Zhou, M. L.; Yao, J. Y.; Lin, Z. S.; Wu, Y. C.; Chen. C. T. *J. Am. Chem. Soc.* **2015**. *137*, 13049.

(26) Zhang. M.;Su, X.; Pan. S. L.; Wang. Z.; Zhang. H.; Yang, Z. H.; Zhang, B. B.; Dong, L. Y.; Wang, Y.; Zhang, F. F.; Yang, Y. *J. Phys. Chem. C* **2014**, *118*, 11849.

(27) Jiang, X. X.; Zhao, S. G.; Lin, Z. S.; Luo, J. H.; Bristowe, P. D.; Guan, X. G.; Chen, C. T. *J. Mater. Chem. C*. **2014**, *2*, 530.